Bull Volcanol (2008) 70:825–840
DOI 10.1007/s00445-007-0172-z

RESEARCH ARTICLE

The "Pomici di mercato" Plinian eruption of Somma-Vesuvius: magma chamber processes and eruption dynamics

M. Aulinas · L. Civetta · M. A. Di Vito · G. Orsi · D. Gimeno · J. L. Férnandez-Turiel

Received: 10 August 2005 / Accepted: 18 September 2007 / Published online: 20 November 2007

Abstract The Pomici di Mercato (PdM, 8,010±40 a), also known in the literature as Pomici Gemelle or Pomici di Ottaviano, is one of the oldest Plinian eruptions of Somma-Vesuvius. This eruption occurred after the longest (7 ka) quiescence period of the volcano and was followed by more than 4 ka of repose. The erupted magma is phonolitic in composition. All the products have very low phenocrysts content (less than 3%) and show evidence of mineralogical disequilibria. They contain K-feldspar ± clinopyroxene (salite and diopside) ± plagioclase ± garnet ± biotite ± amphibole ± apatite ± Fe-Ti oxides. Pumice fragments collected at different stratigraphic heights are slightly less evolved and more enriched in radiogenic Sr composition upsection. The glass composition is fairly homogeneous in single pumice fragment and among pumice fragments from different layers. Glass separated from pumice fragments collected at different stratigraphic heights is homogeneous in the Sr-isotope composition (around a value of 0.70717). Glass is in isotopic equilibrium with salite throughout the entire sequence and with diopside at the base of the sequence. Diopside becomes more radiogenic upsection, reaching a value of 0.707458±7, whereas feldspar is consistently slightly less radiogenic than glass. Nd-isotope composition is fairly uniform (ca. 0.51247) through the whole sequence. The isotopic disequilibria among glass, feldspar and diopside, together with the homogeneous isotopic composition of pumice glass in equilibrium with salite, and the mineralogical disequilibria between plagioclase and K-feldspar, imply that most of the diopside and plagioclase crystals are xenocrysts incorporated into the phonolitic magma during residence in a magma chamber and/or during ascent towards the surface. The PdM Tephra are compositionally and isotopically similar to the phonolitic, first-erupted products of the subsequent Pomici di Avellino Plinian eruption. On the basis of this similarity, we suggest that the magma feeding both eruptions resulted from the tapping of a unique magma chamber. Prior to the PdM eruption, this chamber was formed by a large and homogeneous phonolitic magma body. After the PdM eruption, as a consequence of new arrivals of more radiogenic in Sr, less-differentiated magma batches, the magma chamber progressively developed a slightly stratified phonolitic uppermost portion, capping a tephriphonolitic layer, both emitted during the subsequent Pomici di Avellino eruption.

Keywords Vesuvius · Pomici di Mercato eruption · Magma chamber · Radiogenic isotopes

Editorial responsibility: R. Cioni

M. Aulinas · L. Civetta (✉) · M. A. Di Vito · G. Orsi
Istituto Nazionale di Geofisica e Vulcanologia – Sezione di Napoli - Osservatorio Vesuviano,
via Diocleziano 328,
80124 Naples, Italy
e-mail: civetta@ov.ingv.it

M. Aulinas · D. Gimeno
Universitat Barcelona,
C/ Martí Franquès s/n 08028,
Barcelona, Spain

L. Civetta
Dipt. Science Fisiche, Universitá di Napoli Federico II,
Naples, Italy

J. L. Férnandez-Turiel
Institut of Earth Sciences J. Almera, CSIC,
C/ Lluís Solé i Sabaris,
08028 Barcelona, Spain

Introduction

The Somma-Vesuvius volcano last erupted in 1944, after a period of almost continuous activity that began in AD 1631. The volcano has been quiescent since 1944, apart from fumarolic and moderate seismic activity. Its present state could be interrupted by an eruption with potentially disastrous effects for the 600,000 people living on and around the volcano.

Knowledge of the history and present state of the volcano and its magma feeding system is essential to constrain the most probable maximum and minimum sizes of the next eruption and to recognize its precursors. Most of the petrological investigations of Somma-Vesuvius have been focused on the Pomici di Avellino and Pompei Plinian eruptions, and on the low-energy events of the last century (e.g., Civetta et al. 1991; Civetta and Santacroce 1992; Belkin et al. 1993; Rolandi et al. 1993a; Santacroce et al. 1993; Cioni et al. 1995, Ayuso et al. 1998; Landi et al. 1999; Somma et al. 2001; Marianelli et al. 1995, 2005 and references therein). Much less attention has been paid to the older Plinian eruptions (i.e., Pomici Verdoline and PdM, Fig. 1). In this paper we present new compositional (major and trace elements) and radiogenic isotope data (Nd and Sr) on whole-rock, glass and minerals separates from the PdM Tephra (8,010±40 a, Andronico et al. 1995). This eruption provides a unique opportunity to study the processes active in a magma chamber that fed an eruption preceded by the longest repose time of the volcano (around 7 ka) and followed by about 4 ka of rest. The results of our study evidence a peculiar behaviour of the PdM eruption that, unlike the other Plinian and sub-Plinian Vesuvian eruptions, tapped a homogeneous magma body with no evidence in the erupted products of magma recharge, but rather entrainment of plagioclase and clinopyroxene xenocrysts from the magma chamber walls.

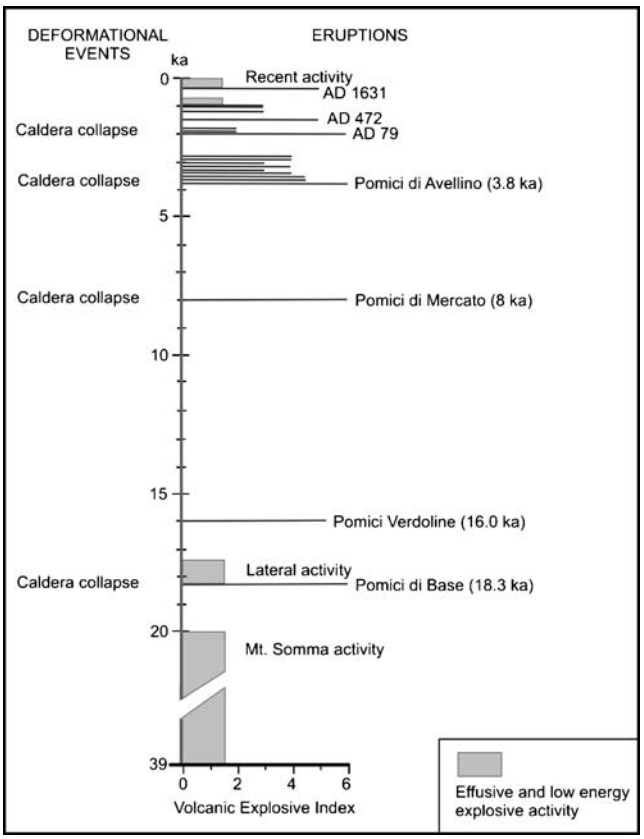

Fig. 1 Chronogram of volcanic and deformational history of Somma-Vesuvius (modified after Santacroce and Sbrana 2003)

Geological outlines

Somma-Vesuvius is a composite central volcano formed by an older stratovolcano (Mt. Somma) whose activity ended with a caldera collapse (Santacroce 1987; Santacroce et al. 2005), and a younger cone (Vesuvius) built inside the caldera (Andronico et al. 1995; Cioni et al. 1999) (Fig. 2). The volcano is located in the Campanian Plain at the intersection of NW-SE and NE-SW-oriented fault systems (Bianco et al. 1998; Ventura and Vilardo 1999).

$^{40}Ar/^{39}Ar$ dating of lavas in cores at 1,125 m b.s.l. indicates that the activity in the Vesuvian area began at about 400 ka (Brocchini et al. 2001), even though the present volcano formed after the Phlegraean Campanian Ignimbrite eruption (39 ka, Orsi et al. 2004 and references therein). The oldest activity of Somma-Vesuvius volcano was mainly characterized by emission of lava flows between 39 and 20 ka. The products of this old activity were recently sampled in a drill hole at Camaldoli della Torre, along the southern slope of the volcano (Di Renzo et al. 2007).

During the last 20 ka, Somma-Vesuvius has been characterized by Plinian and sub-Plinian eruptions, and by periods of semipersistent activity during which lava effusion and low-energy explosive eruptions were typical (Santacroce 1987). The last of such periods followed the AD 1631 eruption and ended with the 1944 eruption. The Pomici di Base (18,300±180 a), PdM (8,010±40 a), Pomici di Avellino (3,780±70 a) and Pomici di Pompei (AD 79) eruptions were Plinian events. The Pomici Verdoline (16,130±110 a), Pollena (AD 472) and AD 1631 eruptions are considered to be sub-Plinian events, as their products are dispersed over smaller areas and the erupted magmas are less voluminous than those of the four Plinian events (Cioni et al. 2003 and references therein). Plinian and sub-Plinian eruptions were preceded by quiescent periods lasting from centuries to millennia. The length of these periods has decreased during the last 3,500 years (Andronico et al. 1995; Cioni et al. 2003).

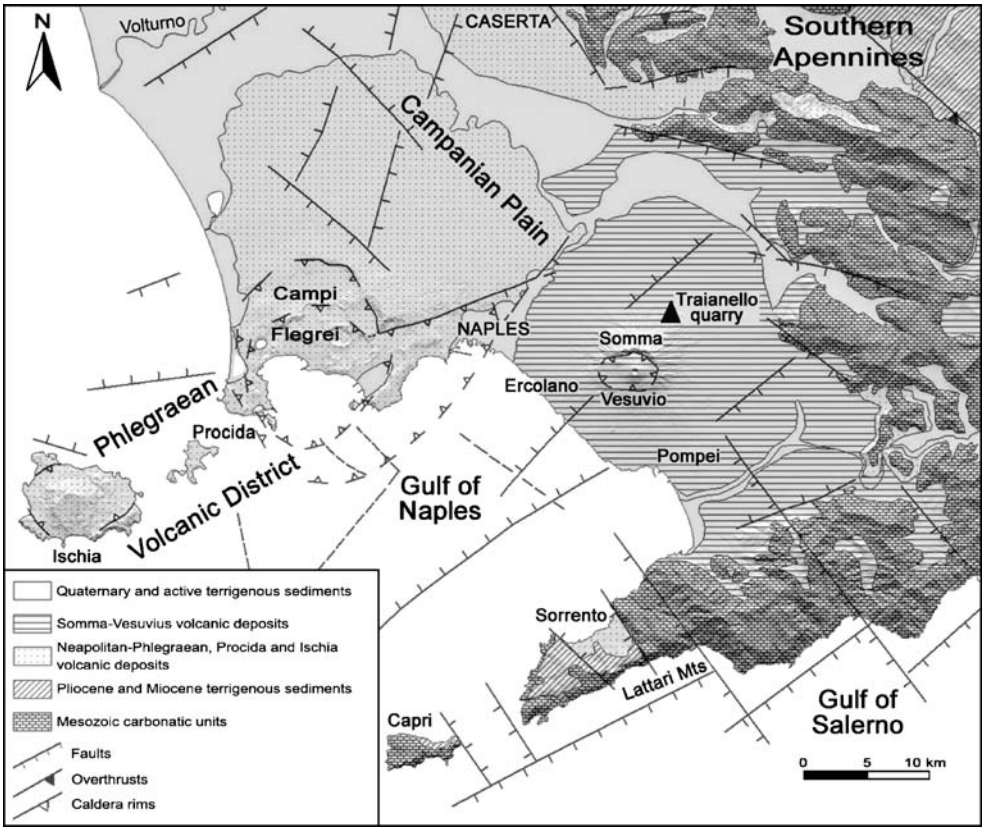

Fig. 2 Geological sketch map of Mt. Vesuvius (modified after Orsi et al. 2004)

The magmatic system of Somma-Vesuvius appears to be characterized by deep and shallow reservoirs. Analyses of melt inclusions in olivine and diopside (Belkin et al. 1985; Marianelli et al. 1995, 1999, 2005; Lima et al. 2003) suggest the existence of a volatile-rich magma storage zone in the crust, discontinuously occurring between 8 and 20 km of depth, where primary magmas crystallize and differentiate. This result agrees with those of a seismic tomography study (Zollo et al. 1996; Auger et al. 2001), which identified a horizontally, regionally extensive low-velocity layer with a flat upper top at about 8 km beneath the volcano. From this reservoir magma rises to form chambers between 8 and 4 km of depth within the Mesozoic carbonate basement, and at shallower depth, before low-energy activity (Santacroce 1983; Santacroce et al. 1993, 1994; Fulignati et al. 1998; Marianelli et al. 1999). The eruptive history of Somma-Vesuvius has been divided into three main periods on the basis of petrological data (Santacroce et al. 1994; Ayuso et al. 1998; Santacroce and Sbrana 2003; Di Renzo et al. 2007). The oldest period (39–9 ka) was characterized by the emission of slightly undersaturated lavas (K-basalt to K-latite) and pyroclastic rocks (K-latite to K-trachyte). In the second period (9 ka–AD 79) the magma composition varied from K-phonolite-tephrite to K-phonolite. The third and youngest period (AD 79–1944) has been characterized by emission of highly undersaturated magmas, from leucititic tephrite to leucititic phonolite (Fig. 3).

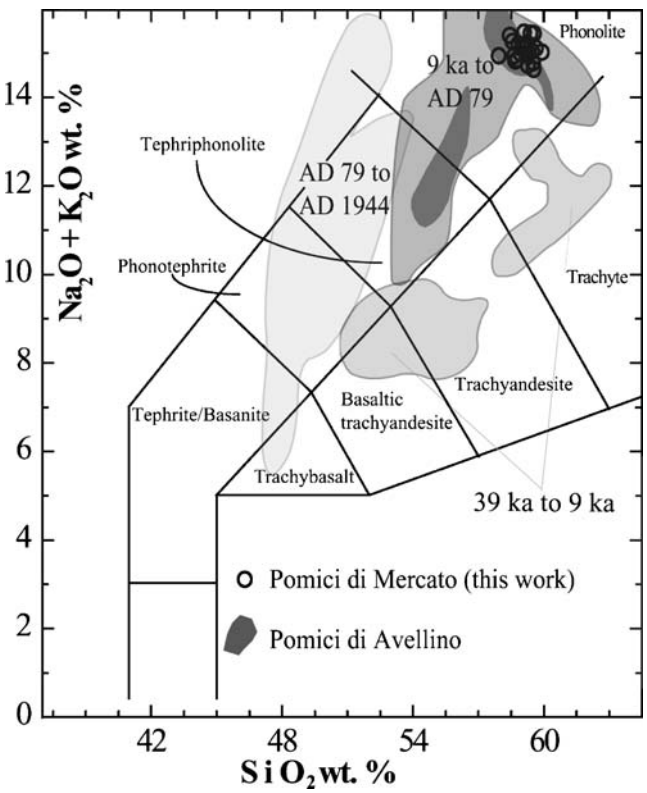

Fig. 3 Total alkali versus silica diagram (TAS) of the three volcanic cycles of Somma-Vesuvius activity, after Santacroce and Sbrana (2003)

Somma-Vesuvius rocks show $^{87}Sr/^{86}Sr$ values ranging from 0.70620 to 0.70810 and $^{143}Nd/^{144}Nd$ ratios ranging from 0.51261 to 0.51238 (Civetta et al. 1987, 1991, 2004; Civetta and Santacroce 1992; Caprarelli et al. 1993; Santacroce et al. 1993; Cioni et al. 1995; Ayuso et al. 1998; Somma et al. 2001; Piochi et al. 2006; Di Renzo et al. 2007). Isotopic data have been largely used to constrain the genesis of the Vesuvius magmas, located in a mantle source variably enriched in sediment derived fluids and melts (e.g., Ayuso et al. 1998; Di Renzo et al. 2007, and references therein). Furthermore, Civetta et al. (2004) and Di Renzo et al. (2007), using isotopic data, suggest that in the "deep" reservoir mantle-derived melts stagnated and were contaminated by crust material, likely a consequence of the high temperatures reached by crustal rocks due to repeated intrusion of magma (de Lorenzo et al. 2006). Magma mixing processes at shallower depth before and/or during eruptions are also well documented by systematic isotopic variations of the magmas emitted during the course of the eruptions and by isotopic mineral disequilibria (Civetta et al. 1991; Civetta and Santacroce 1992; Santacroce et al. 1993; Cioni et al. 1995).

The "Pomici di Mercato" Plinian eruption

The deposits of PdM eruption (8,010±40 a BP, Andronico et al. 1995) were first described by Walker (1977), but subsequently reported as Pomici Gemelle (Delibrias et al. 1979) or Ottaviano eruption (Rolandi et al. 1993b). The stratigraphic sequence of the PdM Tephra has been investigated by many authors. Delibrias et al. (1979) recognized two fallout deposits separated by an ash layer. These fallout deposits are very similar, containing white pumice and small amounts of lithic clasts. Arnó et al. (1987) included in the sequence a third layer previously interpreted as the product of a different eruption, called Pomici e Proietti (Delibrias et al. 1979). Rolandi et al. (1993b) and Cioni et al. (1999 and references therein) reconstructed the eruption history and its physical parameters on the basis of the characteristics of the erupted products. They recognized three fallout layers interbedded in proximal areas with pyroclastic flow and surge deposits. Cioni et al. (1999) interpreted the valley-ponded deposits with breccia lenses, distributed on the northern slopes of the volcano, as related to a syn-eruptive caldera collapse. This collapse affected the northern sector of Monte Somma.

According to the distribution of both fallout and pyroclastic density current deposits, the most complete sequences of the PdM Tephra are exposed in the NE sector of the volcano. In particular the Traianello quarry (Fig. 2), excavated along a paleovalley mainly filled by the PdM Tephra, is the site where the most complete sequence, including widely dispersed fallout and poorly distributed pyroclastic density current deposits, is exposed. The PdM sequence has been reconstructed and described in detail, and the main units have been sampled in the walls of this quarry (Fig. 4). The entire sequence has been subdivided into three members, called A, B, and C from the base upsection. Each member is related to a different eruption phase and includes basal fallout beds overlain by a succession of pyroclastic density current deposits.

According to sedimentological characteristics (Fig. 4), the basal fallout beds of Member A were deposited from a pulsating eruption column that reached a maximum height of 14 km (Rolandi et al. 1993b). The upward increase in lithic content (from 5 to 25%) is probably related to the progressive erosion of the conduit walls (Wilson et al. 1980). The occurrence of interbedded ash layers, together with the faint lamination of the fallout beds, is evidence of an unstable, pulsating column fed by magmatic explosions of variable intensity. Channelling in pre-existing valleys and the occurrence of large clasts suspended in matrix-supported deposits suggest that the pyroclastic density current deposits were laid down by high-density currents, likely produced during partial column collapses. In mid-distal areas the fallout deposits are overlain only by a thin ash fallout (Arnò et al. 1987; Rolandi et al. 1993b), which is probably due to late deposition of fine particles during or after the destabilization of the column.

Member B conformably overlies the upper pyroclastic density current deposits of Member A (Fig. 4). The faintly stratified, Member B basal fallout deposits were generated by a pulsating column, which reached a maximum height of 20 km (Rolandi et al. 1993b). The interbedded thin ash layer, distributed both in proximal and in mid-distal areas, is interpreted as a lower-energy phase of the eruption. The surge beds widely distributed along the northern slopes of Mt. Somma, described also in Rolandi et al. (1993b), are evidence of phreatomagmatic explosions during a dominantly magmatic phase of the eruption. This phase of activity also featured an unstable column that partially collapsed to produce dense pyroclastic currents. The distribution of pyroclastic density currents was strongly controlled by the pre-existing topography (Rolandi et al. 1993b; Cioni et al. 1999). The intimate alternation of fallout and flow deposits could be taken as an indication that the unstable column was affected by many collapse episodes.

Member C conformably overlies Member B (Fig. 4). The stratified basal fallout beds of this member were deposited by a pulsating and unstable column that reached a maximum height of 22 km (Rolandi et al. 1993b). The upper pyroclastic-current deposits, which are the last of the PdM eruption, are confined to pre-existing valleys and were very likely generated by density currents that resulted from the collapse of the eruption column. The occurrence of lithic fragments, almost exclusively lava fragments, and

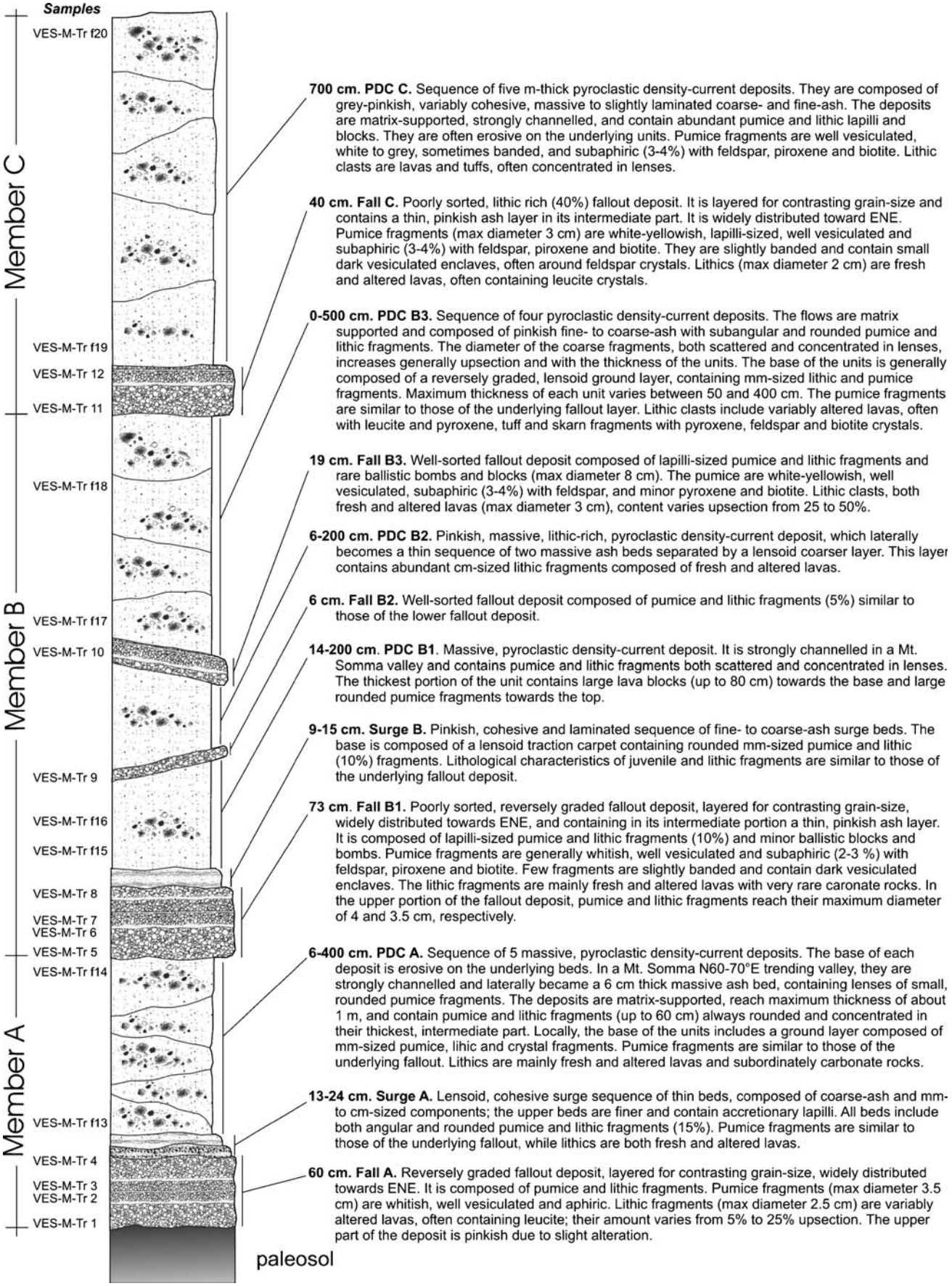

Fig. 4 Type section of the Pomici di Mercato Tephra. The main characteristics of the erupted sequence as well as the sampled layers are reported

Table 1 Selected analyses of sanidine from Pomici di Mercato Tephra

Sample	VES-M TR1	VES-M TR2	VES-M TR3	VES-M TR4	VES-M TR5	VES-M TR6	VES-M TR6	VES-M TR7B	VES-M TR8	VES-M TR9	VES-M TR11	VES-M TRf13	VES-M TRf14	VES-M TRf15	VES-M TRf19
Layer	Fall A	Fall A	Fall A	Fall A	Fall B1	Fall B1	Fall B1	Fall B1	Fall B1	Fall B2	Fall C	PDC A	PDC B1	PDC B1	PDC C
%															
SiO_2	64.98	64.99	65.4	64.81	64.92	64.8	64.9	65.41	64.94	65.04	62.64	65.31	65.56	65.62	65.56
TiO2	0.01	0.01	0.03	0.03	0.04	0.01	0.03	0.03	0.03	0.02	0.04	0.01	0.04	0.01	0.01
Al_2O_3	18.98	19.23	19.23	19.31	19.25	19.67	19.67	19.10	19.21	19.5	20.39	19.08	18.83	18.91	18.79
MgO	<0.01	0.02	0.01	<0.01	0.01	<0.01	0.06	<0.01	0.01	<0.01	<0.01	<0.01	<0.01	<0.01	<0.01
CaO	0.27	0.29	0.32	0.32	0.33	0.37	0.28	0.33	0.03	0.26	1.49	0.38	0.38	0.32	0.34
MnO	<0.01	0.03	<0.01	0.02	<0.01	0.01	<0.01	0.02	<0.01	<0.01	<0.01	<0.01	<0.01	<0.01	0.03
FeO	0.17	0.2	0.13	0.19	0.17	0.13	0.21	0.17	0.13	0.14	0.27	0.23	0.1	0.12	0.17
Na_2O	3.67	3.55	3.58	3.6	3.82	3.76	3.46	3.95	3.88	3.98	2.67	3.68	3.68	3.65	4.01
K_2O	11.48	11.37	11.23	11.2	11.03	11.02	11.13	11.06	11.2	10.99	11.49	11.37	11.17	11.29	10.91
SrO	0.06	<0.01	0.09	<0.01	0.11	0.13	<0.01	0.08	0.05	<0.01	0.13	<0.01	<0.01	<0.01	<0.01
BaO	<0.01	<0.01	0.03	<0.01	0.00	0.05	<0.01	0.03	0.03	0.01	2.67	<0.01	0.03	<0.01	<0.01
Total	99.62	99.7	100.05	99.49	99.71	99.95	99.18	100.17	99.82	99.95	99.15	100.13	99.78	99.92	99.85
%															
ab	32.27	31.7	32.1	32.31	33.92	33.48	31.66	34.62	33.92	35.02	24.12	32.5	32.74	32.42	35.7
or	66.43	66.89	66.26	66.11	64.46	64.61	66.91	63.75	64.44	63.68	68.38	65.7	65.33	65.19	62.37
an	1.3	1.4	1.59	1.58	1.62	1.81	1.43	1.59	1.59	1.29	7.46	1.85	1.89	1.59	2.04

PDC Pyroclastic density current

Table 2 Selected analyses of plagioclase from Pomici di Mercato Tephra

Sample	VES-M TR1	VES-M TR2	VES-M TR3	VES-M TR6	VES-M TR6	VES-M TR6	VES-M TR7	VES-M TR7	VES-M TRf14	VES-M TRf16	VES-M TRf16	VES-M TRf20	VES-M TRf20
Layer	Fall A	Fall A	Fall A	Fall B1	Fall B1	Fall B1	Fall B1	Fall B1	PDC A	PDC B	PDC B	PDC C	PDC C
%													
SiO_2	62.63	62.93	62.48	62.33	62.3	62.5	64.85	62.37	62.69	63.53	63.15	62.75	63.01
TiO_2	0.01	0.01	<0.01	0.01	0.04	<0.01	0.01	<0.01	0.01	0.02	0.03	<0.01	<0.01
Al_2O_3	23.05	23.09	23.3	22.97	23.52	23.21	23.2	22.76	22.94	22.87	22.5	22.5	22.69
MgO	0.01	0.09	<0.01	<0.01	<0.01	<0.01	<0.01	<0.01	<0.01	0.01	<0.01	<0.01	<0.01
CaO	4.2	4.03	4.26	3.92	4.55	4.26	4.33	4.04	4.23	4.31	3.92	3.8	4.14
MnO	<0.01	0.01	<0.01	0.01	0.00	0.06	0.01	<0.01	<0.01	<0.01	<0.01	<0.01	<0.01
FeO	0.31	0.27	0.196	0.24	0.25	0.24	0.2	0.26	0.25	0.23	0.19	0.23	0.18
Na_2O	8.26	8.51	8.32	8.34	8.71	8.15	8.89	8.7	8.36	8.1	8.57	8.32	8.17
K_2O	1.46	1.38	1.38	1.64	1.35	1.37	1.43	1.43	1.37	1.37	1.56	1.53	1.38
SrO	0.11	0.07	<0.01	<0.01	<0.01	<0.01	<0.01	<0.01	<0.01	<0.01	<0.01	<0.01	<0.01
BaO	0.03	0.02	<0.01	<0.01	<0.01	<0.01	<0.01	<0.01	<0.01	<0.01	<0.01	<0.01	<0.01
Total	100.07	100.40	99.94	99.95	100.72	99.81	99.92	99.58	99.84	100.45	99.96	99.13	99.72
%													
ab	71.52	73.08	71.84	72.01	71.91	71.44	72.72	73.24	72.11	71.18	72.78	72.5	71.98
or	8.34	7.78	7.85	9.3	7.33	7.92	7.7	7.95	7.75	7.89	8.84	7.76	8.2
an	20.08	19.11	20.31	18.69	20.76	20.65	19.57	18.81	20.14	20.93	18.39	18.94	19.13

PDC Pyroclastic density current

their increase throughout the entire sequence of the PdM, but mainly in Member C, suggests a progressive enlargement by abrasion and/or collapse of the conduit due to magma pressure variation. The latter mechanism is also supported by the instability of the eruption column, which reached its maximum height during the deposition of Member C (Rolandi et al. 1993b). Enlargement of the conduit favored increases in both the magma discharge rate and the eruption column height.

A detailed mineralogical, geochemical, and isotopic characterization of the products of the PdM eruption is still lacking in the literature. Joron et al. (1987) reported compositional data (major and trace elements) for a few samples from this eruption and Ayuso et al. (1998) and Scheibner et al. (2007) reported isotopic data for whole-rocks and minerals of few samples of PdM Tephra. Mineral analyses were reported by Joron et al. (1987), Rolandi et al. (1993b) and Scheibner et al. (2007).

Sampling and analytical methods

Twenty samples representative of the different units were collected from this stratigraphic section. Multiclast pumice samples, single pumice, and separated minerals were analyzed for major and trace elements, mineral chemistry and Sr and Nd isotopic compositions.

Whole-rock XRF (X-Ray fluorescence) major and trace elements analyses (except REE, Hf and Th) were performed using a sequential X-ray spectrometer Philips PW2400 at Serveis Cientifico Tecnics (SCT), University of Barcelona. REE, Th, Ta, and Hf were also analyzed by ICP-MS (inductively coupled plasma-mass spectrometry) at the SCT. Accuracy was checked against international standards provided by the Geological Survey of Japan (GSJ JA-2 for major elements and JB-3 for REE, Th and Hf analyzed by ICP-MS) and by the University of Barcelona (GSS-8 for trace elements analyzed by XRF). The precision was 3% (1σ) for major elements and 1–5% (1σ) for trace elements.

Sr and Nd isotopes were determined at the Istituto Nazionale di Geofisica e Vulcanologia - Osservatorio Vesuviano, Naples, Italy, using a multicollector Finnigan-Triton TI Mass Spectrometer. Sr isotopes were measured on 15 whole-rock samples and 20 separated minerals (feldspar, salite, diopside). Glass was analyzed for four single and four composite pumice samples. Nd isotopes were determined on seven whole-rock samples. Isotopes were separated using the standard cation-exchange chromatographic technique. Analyses of La Jolla standard gave an average for $^{143}Nd/^{144}Nd=0.511846\pm0.000015$ (2σ, number of standard analyses=25). Analyses of NIST SRM-987 gave $^{87}Sr/^{86}Sr=0.710253\pm0.000014$ (2σ, number of standard analyses=56), where 2σ represents the external reproducibility, according to Deines et al. (2003). The Sr and Nd blanks were negligible for the analyzed samples during the period of measurements.

Selected samples (glass and phenocrysts) were studied by EMPA (electron microprobe analysis) at the SCT. Glasses and phenocrysts were analyzed using a Cameca SX-50 with a configuration made of four WDS and one EDS spectrometers. The instrument was calibrated with commercial standards (natural silicates and oxides with certified composition). The analytical routine of the program used was the one described by Díaz et al. (1996).

Petrography and mineral chemistry

All studied rocks are aphanitic, glassy pumice. All samples show hypocrystalline textures with rare phenocrysts ranging from 1 to 3% in a glassy to cryptocrystalline vesiculated matrix. In some cases sanidine crystals form a glomeroporphyric texture.

The main phases are: K-feldspar, clinopyroxene, plagioclase, garnet, biotite, amphibole, and accessory apatite and Fe-Ti oxides. Joron et al. (1987) reported nepheline as a mineral phase in the PdM deposits. Although nepheline was

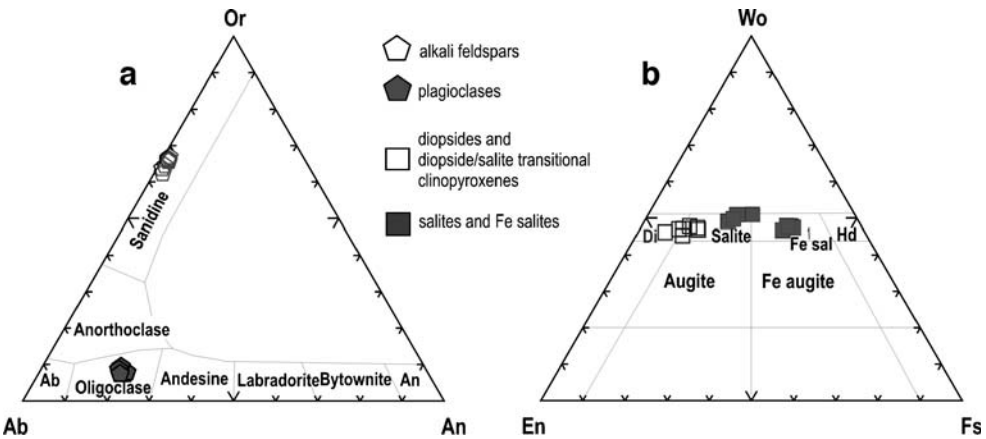

Fig. 5 Classification of Pomici di Mercato feldspars (**a**) and clinopyroxenes (**b**)

Table 3 Selected analyses of clinopyroxene from Pomici di Mercato Tephra

Sample	VES-M TR6	VES-M TR6	VES-M TR7	VES-M TR8	VES-M TR8	VES-M TR11	VES-M TR11	VES-M TR11	VES-M TRf13	VES-M TRf15	VES-M TRf15	VES-M TRf15	VES-M TRf15	VES-M TRf18	VES-M TRf20
Layer	Fall B1	Fall B1	Fall B1	Fall B1	Fall B1	Fall C	Fall C	Fall C	PDC A	PDC B1	PDC B1	PDC B1	PDC B1	PDC B2	PDC C
%															
SiO_2	43.65	45.03	45.31	43.20	45.70	45.84	48.24	48.19	47.51	50.59	41.50	53.91	50.94	49.35	45.57
TiO_2	1.59	1.33	1.32	1.12	0.59	0.72	1.34	1.12	1.44	0.83	1.87	0.34	0.44	1.02	0.56
Al_2O_3	8.42	7.39	7.09	6.49	4.90	5.52	5.58	6.24	7.21	3.55	10.55	1.39	2.23	5.72	3.71
Fe_2O_3	7.16	7.07	6.89	11.27	9.42	6.24	4.21	3.84	4.06	2.54	8.82	1.25	4.48	3.07	8.85
MgO	9.16	10.37	9.76	5.32	6.18	5.52	13.18	13.89	13.2	15.29	7.84	17.43	15.84	14.89	5.27
CaO	23.13	22.83	23.01	21.13	20.84	20.81	22.25	22.69	21.96	22.01	22.82	23.61	23.68	22.81	21.22
MnO	0.23	0.25	0.30	1.37	1.51	1.24	0.24	0.12	0.25	0.17	0.22	0.2	0.14	0.14	1.83
FeO	5.60	5.20	5.83	8.53	9.50	12.27	4.11	3.34	4.5	4.42	6.01	2.88	1.81	3.38	10.91
Na_2O	0.39	0.40	0.50	1.33	1.38	1.16	0.54	0.29	0.36	0.26	0.38	0.08	0.17	0.30	1.22
K_2O	<0.01	<0.01	0.01	<0.01	<0.01	<0.01	<0.01	<0.01	0.01	<0.01	0.03	<0.01	<0.01	<0.01	<0.01
Total	99.33	99.87	100.03	99.77	100.03	99.34	99.72	99.73	100.5	99.65	100.04	101.1	99.72	100.08	99.15
%															
wo	50.89	49.12	49.79	47.82	46.66	47.92	47.40	47.86	46.84	45.24	50.95	46.17	47.00	47.10	47.44
en	28.03	31.04	29.38	16.75	19.25	17.68	39.06	40.76	39.17	43.72	24.35	47.41	43.73	42.77	16.39
fs	21.08	19.84	20.83	35.43	34.09	34.40	13.54	11.39	14.00	11.03	24.69	6.42	9.27	10.13	36.17

PDC Pyroclastic density current

Table 4 Selected analyses of glass from Pomici di Mercato Tephra

Sample	VES-M TR2	VES-M TR2	VES-M TR4	VES-M TR4	VES-M TR6	VES-M TR6	VES-M TR7	VES-M TR7	VES-M TR8	VES-M TR9	VES-M TR9	VES-M TR9
Layer	Fall A	Fall A	Fall A	Fall A	Fall B1	Fall B1	Fall B1	Fall B1	Fall B1	Fall B2	Fall B2	Fall B2
%												
SiO_2	58.87	59.22	59.34	58.90	59.19	59.41	59.55	59.44	59.80	58.85	59.45	59.58
TiO_2	0.12	0.12	0.13	0.09	0.11	0.13	0.13	0.11	0.10	0.14	0.13	0.13
Al_2O_3	22.99	22.65	22.12	22.83	22.31	22.97	21.74	21.01	21.15	21.81	21.15	21.43
MgO	0.05	0.07	0.07	0.03	0.03	0.04	0.06	0.10	0.06	0.10	0.06	0.09
CaO	1.50	1.54	1.60	1.63	1.55	2.35	1.63	1.68	1.74	1.59	1.69	1.63
MnO	0.18	0.17	0.22	0.19	0.14	0.13	0.18	0.22	0.17	0.14	0.16	0.19
FeO	1.84	1.87	1.86	1.93	1.74	1.65	1.75	1.78	1.79	1.82	1.87	1.81
Na_2O	8.19	8.20	8.38	7.82	8.70	8.03	8.59	9.06	8.49	9.08	8.90	8.89
K_2O	6.26	6.16	6.28	6.58	6.23	5.29	6.38	6.60	6.71	6.47	6.59	6.25

Table 5 Major oxide (%) and trace element concentration (ppm), differentiation index (DI) and CIPW norm (according with Middlemost 1989) of Pomici di Mercato Tephra

Sample	VES-M TR1	VES-M TR2	VES-M TR3	VES-M TR4	VES-M TR5	VES-M TR6	VES-M TR6B	VES-M TR7	VES-M TR7B	VES-M TR8	VES-M TR9	VES-M TR10	VES-M TR11	VES-M TR12	VES-M TRf13	VES-M TRf14	VES-M TRf15	VES-M TRf16	VES-M TRf17	VES-M TRf18	VES-M TRf19	VES-M TRf20
Layer	Fall A	Fall A	Fall A	Fall A	Fall B1	Fall B1	Fall B1	Fall B1	Fall B1	Fall B1	Fall B2	Fall B3	Fall C	Fall C	PDC A	PDC A	PDC B1	PDC B1	PDC B2	PDC B2	PDC C	PDC C
SiO_2	56.84	56.78	57.02	56.99	56.92	56.15	56.68	56.17	57.50	56.03	57.03	56.42	55.99	56.49	56.70	56.28	56.24	56.11	57.51	57.20	56.20	56.45
TiO_2	0.04	0.04	0.08	0.10	0.03	0.11	0.12	0.13	0.13	0.14	0.13	0.15	0.17	0.17	0.09	0.13	0.15	0.15	0.16	0.16	0.15	0.15
Al_2O_3	20.06	20.19	20.10	19.88	20.02	20.00	20.24	20.29	21.25	19.93	20.52	20.36	20.57	20.33	20.08	20.18	19.99	20.11	20.60	20.44	20.30	20.14
Fe_2O_3	1.82	1.80	1.88	1.93	1.81	1.95	2.02	2.12	2.21	2.06	2.12	2.10	2.21	2.22	1.93	2.00	2.10	2.11	2.21	2.18	2.08	2.14
MnO	0.17	0.17	0.17	0.18	0.16	0.17	0.17	0.17	0.18	0.17	0.17	0.17	0.16	0.16	0.17	0.18	0.17	0.18	0.17	0.18	0.17	0.17
MgO	0.05	0.05	0.04	0.11	0.08	0.08	0.17	0.20	0.19	0.09	0.12	0.14	0.20	0.20	0.11	0.11	0.13	0.15	0.17	0.20	0.13	0.16
CaO	1.49	1.46	1.54	2.17	1.73	1.97	1.97	1.81	1.91	1.74	1.79	1.84	1.99	1.97	1.79	1.79	1.76	1.77	1.95	2.07	1.80	1.75
Na_2O	8.12	7.98	8.13	7.91	7.76	7.81	7.52	7.78	7.92	7.74	7.35	7.32	7.20	7.19	7.70	7.70	7.59	7.72	7.25	7.45	7.66	7.33
K_2O	6.54	6.65	6.60	6.61	6.56	6.72	6.54	6.49	6.62	6.86	7.01	6.89	7.01	6.97	6.68	6.81	6.90	6.93	7.06	7.06	6.86	6.77
P_2O_5	0.01	0.01	0.01	0.01	0.01	0.01	0.03	0.03	0.03	0.02	0.02	0.02	0.03	0.03	0.02	0.02	0.02	0.02	0.03	0.03	0.03	0.02
LOI	3.95	4.10	3.76	3.25	3.90	4.05	3.76	3.88	3.00	4.29	3.56	3.65	3.37	3.35	3.86	3.59	3.78	3.84	3.34	3.54	3.57	4.11
Total	99.09	99.23	99.33	99.14	98.98	99.02	99.22	99.07	100.94	99.07	99.82	99.06	98.90	99.08	99.13	98.79	98.83	99.09	100.45	100.51	98.95	99.19
DI	92.24	93.20	92.01	90.77	92.78	91.81	90.65	91.28	90.24	91.70	91.01	90.76	89.69	90.04	92.33	92.26	92.31	91.93	90.17	90.65	91.88	90.99
Ortoclase	40.62	41.31	40.81	40.73	40.77	41.81	40.48	40.29	39.94	42.77	43.03	42.67	43.36	43.02	41.43	42.27	42.90	42.99	42.96	43.02	42.50	42.07
Albite	29.68	30.19	29.31	28.50	31.86	27.61	30.68	29.53	28.87	26.55	28.32	28.20	25.70	27.46	30.22	28.18	27.95	26.31	28.35	27.09	27.43	29.63
Anortite	0.00	0.00	0.00	0.00	0.44	0.00	2.26	1.34	2.94	0.00	2.39	2.46	3.25	2.73	0.52	0.41	0.10	0.00	2.90	1.53	0.78	2.16
Nepheline	21.94	21.70	21.90	21.54	20.15	22.38	19.49	21.46	21.42	22.38	19.66	19.89	20.62	19.55	20.67	21.81	21.46	22.63	18.86	20.54	21.95	19.28
Acmite	1.72	0.64	1.77	1.36	0.00	0.58	0.00	0.00	0.00	1.09	0.00	0.00	0.00	0.00	0.00	0.00	0.00	0.43	0.00	0.00	0.00	0.00
Diopside	4.88	4.27	4.80	5.02	4.10	4.44	4.70	5.03	5.02	4.87	4.53	4.58	5.00	5.01	4.32	4.35	4.54	4.93	4.82	4.98	4.49	4.78
Wollast.	0.91	1.13	1.05	2.27	1.60	2.16	0.98	0.86	0.31	1.43	0.63	0.71	0.45	0.62	1.55	1.59	1.56	1.43	0.54	1.29	1.34	0.55
Magnetite	0.00	0.53	0.00	0.23	0.86	0.63	0.95	1.00	1.02	0.43	0.99	0.99	1.04	1.04	0.91	0.95	0.99	0.78	1.02	1.01	0.98	1.01
Ilmenite	0.08	0.08	0.16	0.20	0.06	0.22	0.24	0.26	0.25	0.28	0.26	0.30	0.34	0.34	0.18	0.26	0.30	0.30	0.31	0.31	0.30	0.30
Apatite	0.02	0.02	0.02	0.02	0.02	0.02	0.07	0.07	0.07	0.05	0.05	0.05	0.07	0.07	0.05	0.05	0.05	0.05	0.07	0.07	0.07	0.05
Ba	41	48	40	4	10	27	32	8	14	12	54	78	104	102	10	4	47	37	82	45	61	60
Co	0.1	2.0	0.3	0.5	1.9	1.6	0.5	2.1	0.5	0.3	1.4	1.0	0.7	1.7	0.2	0.4	0.3	0.1	1.1	0.1	1.3	0.2
Cr	14	15	16	17	16	15	22	18	17	16	14	16	14	15	13	13	14	13	14	14	15	13
Cu	1.1	1.5	1.8	0.5	0.5	1.7	0.5	1.3	0.6	0.7	0.1	0.6	0.5	0.1	0.2	0.3	0.1	0.1	0.7	0.1	0.1	0.2
Ga	29	27	28	28	28	27	27	27	27	26	27	26	26	25	27	26	27	27	26	26	27	27
Hf	18	17	17	17	18	17	15	16	15	16	16	15	14	14	17	19	15	15	16	19	16	15
Mo	3.1	2.9	3.7	3.7	3.9	3.5	3.7	3.2	3.9	4.5	4.5	5.0	4.7	5.3	3.9	3.2	4.7	4.8	5.0	4.6	5.2	5.3
Nb	95	91	94	92	92	88	87	89	87	84	86	83	83	81	89	87	89	88	85	86	91	88
Ni	1.1	2.2	1.3	1.3	1.2	1.8	1.3	1.7	0.9	1.9	1.0	1.6	0.7	0.8	0.5	0.6	0.4	0.5	0.7	0.6	0.8	0.5
Pb	126	120	123	121	120	115	115	115	115	110	111	108	105	102	117	115	114	113	109	110	117	113
Rb	558	531	548	536	539	519	502	519	484	494	510	495	492	481	523	509	524	518	502	506	524	510
Sn	1.3	1.6	1.5	1.7	4.2	2.7	2.7	3.1	2.8	1.6	4.4	2.8	3.5	2.3	3.9	0.7	2.5	2.2	2.8	3.0	3.1	4.2
Sr	22	20	29	39	41	41	56	46	60	55	81	98	131	130	44	40	71	75	103	85	82	80
Ta	1.1	1.4	0.5	1.1	1.9	1.5	1.6	1.6	0.9	1.6	2.0	1.4	2.1	2.1	2.1	1.8	1.6	1.8	1.7	1.9	2.0	1.2
Th	96	90	92	91	90	87	85	87	85	84	83	80	78	77	89	85	87	86	81	83	87	85
V	15	15	16	17	17	17	20	18	21	18	21	22	25	25	18	18	20	21	23	21	20	21

Table 5 (continued)

Sample	VES-M TR1	VES-M TR2	VES-M TR3	VES-M TR4	VES-M TR5	VES-M TR6	VES-M TR6B	VES-M TR7	VES-M TR7B	VES-M TR8	VES-M TR9	VES-M TR10	VES-M TR11	VES-M TR12	VES-M TRf13	VES-M TRf14	VES-M TRf15	VES-M TRf16	VES-M TRf17	VES-M TRf18	VES-M TRf19	VES-M TRf20
Layer	Fall A	Fall A	Fall A	Fall A	Fall B1	Fall B1	Fall B1	Fall B1	Fall B1	Fall B1	Fall B2	Fall B3	Fall C	Fall C	PDC A	PDC A	PDC B1	PDC B1	PDC B2	PDC B2	PDC C	PDC C
W	16	15	16	16	17	16	16	15	15	15	15	14	15	15	15	16	16	16	16	16	16	16
Y	8.7	7.9	9.1	9.1	9.0	8.4	9.2	9.6	9.8	9.0	11	11	12	12	10	9.2	12	12	12	12	11	11
Zn	153	147	150	148	148	142	141	143	142	137	139	135	133	130	146	141	145	143	137	139	143	140
Zr	905	862	883	863	859	825	812	827	817	782	795	761	743	727	839	814	823	816	776	792	819	809
La	74	59	70	102	71	96	89	81	59	100	97	100	88	87	91	43	73	74	63	64	91	63
Ce	137	121	155	181	142	172	159	150	126	170	174	174	154	156	187	101	174	160	148	157	183	135
Pr	12	10	12	17	13	16	15	14	11	16	16	17	16	15	15	7	12	12	11	12	15	12
Nd	34	28	33	47	36	45	42	38	31	46	46	48	45	44	42	21	34	37	33	35	44	35
Sm	4.0	3.2	4.0	5.5	4.3	5.2	4.9	4.6	3.8	5.5	5.7	6.0	5.8	5.8	4.7	2.3	4.0	4.4	4.1	4.5	5.1	4.7
Eu	0.4	0.4	0.5	0.6	0.5	0.7	0.6	0.6	0.5	0.7	0.8	0.8	0.9	0.9	0.6	0.3	0.5	0.6	0.6	0.7	0.7	0.6
Gd	4.4	3.6	4.4	5.9	4.5	5.7	5.3	5.0	4.1	6.0	6.2	6.2	6.1	5.9	5.6	2.8	4.8	5.2	4.7	5.1	5.7	4.9
Tb	0.4	0.3	0.4	0.5	0.4	0.5	0.5	0.5	0.4	0.6	0.6	0.6	0.6	0.6	0.5	0.2	0.4	0.5	0.5	0.5	0.5	0.5
Dy	1.7	1.4	1.8	2.3	2.0	2.3	2.2	2.0	1.9	2.4	2.6	2.6	2.7	2.7	2.0	1.1	1.9	2.2	2.0	2.3	2.4	2.4
Ho	0.3	0.3	0.3	0.4	0.4	0.4	0.4	0.4	0.4	0.5	0.5	0.5	0.5	0.5	0.4	0.2	0.4	0.4	0.4	0.4	0.4	0.5
Er	1.0	0.9	1.1	1.4	1.2	1.3	1.3	1.2	1.2	1.4	1.5	1.6	1.6	1.6	1.2	0.7	1.1	1.4	1.3	1.5	1.5	1.4
Tm	0.2	0.2	0.2	0.2	0.2	0.2	0.2	0.2	0.2	0.2	0.3	0.3	0.3	0.2	0.2	0.1	0.2	0.2	0.2	0.2	0.2	0.2
Yb	1.3	1.1	1.4	1.6	1.5	1.6	1.5	1.4	1.4	1.7	1.8	1.8	1.8	1.8	1.4	0.9	1.4	1.6	1.5	1.8	1.6	1.7
Lu	0.2	0.2	0.2	0.3	0.2	0.3	0.2	0.2	0.2	0.3	0.3	0.3	0.3	0.3	0.2	0.1	0.2	0.3	0.3	0.3	0.3	0.3

PDC Pyroclastic density current

not found in any of the studied thin sections, CIPW norms for whole-rocks are nepheline-normative, with ne=18–23%.

Feldspars: Sanidine, the most abundant mineral in all samples, occurs as phenocrysts, microphenocrysts, and microlites in the groundmass in all the studied samples. The crystals are predominantly euhedral, only a few are moderately rounded. The single crystals generally have a homogeneous composition of $Or_{62–70}$ (Table 1). Plagioclase, occasionally occurring as euhedral microphenocrysts, is generally rounded, very homogeneous, without zoning, and ranges in composition between An_{20} and An_{25} (Table 2). Inspection of Fig. 5a clearly shows that plagioclase and sanidine are not in equilibrium as K-feldspar of $Or_{62–70}$ would be in equilibrium with a plagioclase $An_{>70}$. Furthermore, the rounded shape of some plagioclase crystals agrees with their disequilibrium in the liquid.

Clinopyroxene: Pyroxene occurs as greenish salite and colorless diopside euhedral phenocrysts, both fairly homogeneous in composition. Salite composition is $Wo_{46–51}$-$En_{16–31}$-$Fs_{19–36}$. Diopside is quite homogeneous $Wo_{45–47}$-$En_{39–47}$-$Fs_{6–13}$ (Table 3). The clinopyroxene classification diagram (Fig. 5b) shows that many diopsides plot close to the salitic field and the occurrence of two different groups of salites and Fe-salites. This compositional variation is not related to the stratigraphic position of the analyzed sample, as diopside, salite and Fe-salite occur over all the stratigraphic sequence.

Garnet: Garnet is a common phase in all samples and occurs as idiomorphic orange-brownish phenocrysts. It is unzoned and has abundant sanidine and some minor inclusions of clinopyroxene, titanite, apatite. According to the detailed geochemical study of Scheibner et al. (2007), PdM garnets are of magmatic origin and are Ti- and Fe-rich andradites, with small variation in their Al-Fe-content between $Gro_{31}And_{69}$ and $Gro_{33}And_{67}$.

Other mineral phases: Mineral phases such as amphibole, apatite, and Fe-oxides have been found as inclusions in other minerals and as microphenocrysts too small to be analysed. Rolandi et al. (1993b) stated that amphibole from the PdM products has an almost constant calcic composition and can be classified as pargasite-hastingsite. Biotite is rarely present in these samples. It only occasionally occurs as idiomorphic microphenocryst.

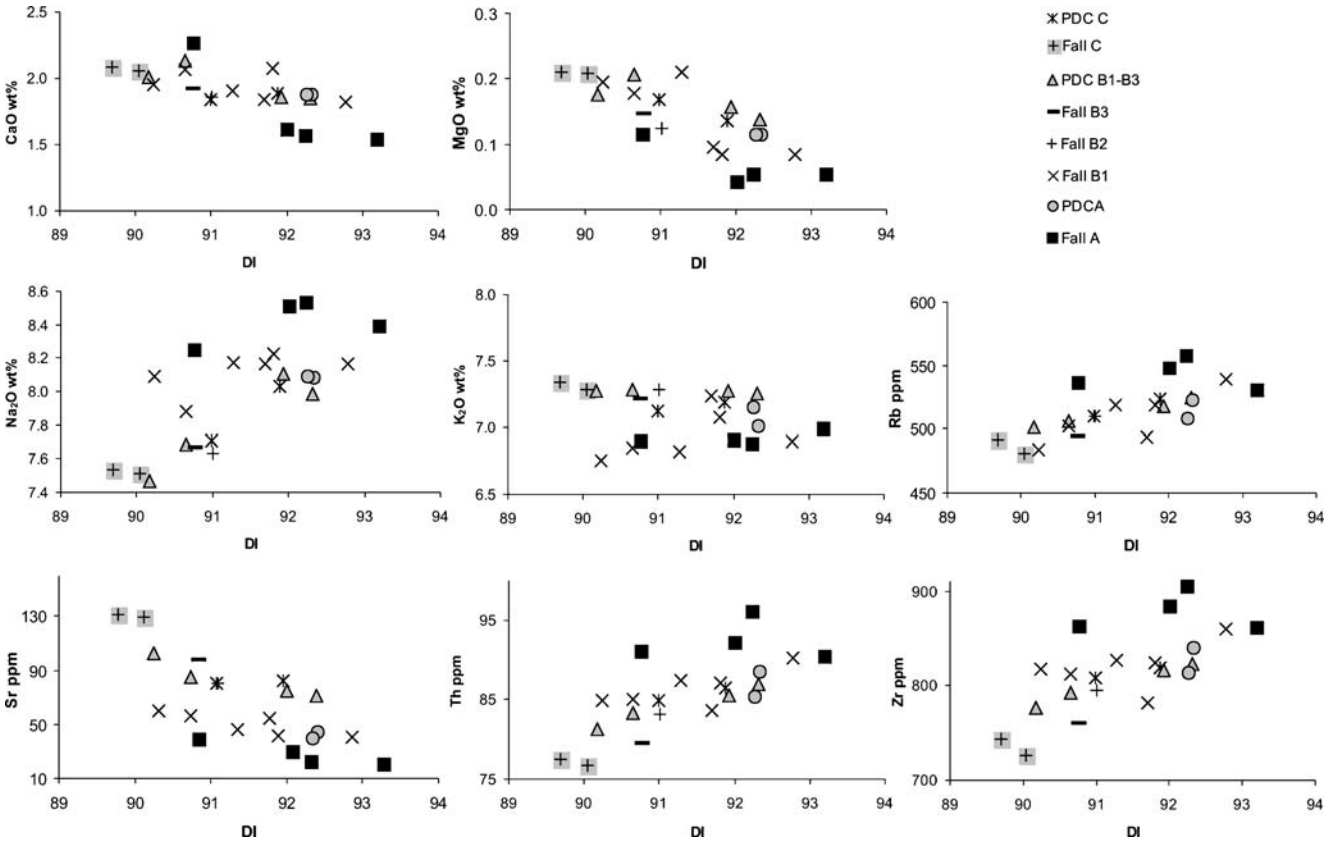

Fig. 6 Pomici di Mercato variation diagrams for representative major (wt%) and trace (ppm) elements versus DI (Differentiation Index, Thornton and Tuttle 1960)

Glass composition: Due to the high vesicularity of all the samples and the extreme thinness of the glass shards and vesicles walls, glass analyses have been problematic and only a few data are reported in Table 4. Analyses were performed on pumice clasts from several stratigraphic levels. All the analyzed samples show a fairly uniform composition (CaO~1.6wt%; Na2O~8.1wt%; K2O~7wt%). Glass compositions are similar to those of the whole rocks.

Chemistry and Sr and Nd radiogenic isotopes

Whole-rock compositions Major and trace element contents as well as the CIPW norms of the analyzed samples are presented in Table 5. In the TAS classification diagram (Le Bas et al. 1989) (Fig. 3) all samples fall in the phonolitic field. They are nepheline normative and range in DI (Differentiation Index, Thornton and Tuttle 1960) from 89 to 93. These results are in full agreement with those reported by Joron et al. (1987), even though our silica values are slightly higher.

Plots of major and trace element contents versus DI for whole-rock pumice samples (Fig. 6) show regular, though very restricted, variations. MgO, CaO, K_2O, FeO_{tot} and TiO_2 show an inverse correlation with DI. On the other hand, Na_2O shows a positive correlation with DI, while SiO_2 and Al_2O_3 remain fairly constant at varying DI. Rb, Th, Nb, Zr, Ta, Hf and REE slightly increase at increasing DI, whereas Sr, Ba, V, Cr, Co and Ni are negatively correlated with DI. Although major and trace element variations for all samples are limited, the general trend is towards less evolved magma composition with increasing stratigraphic height (Fig. 7), with the exception of the uppermost pyroclastic density current products, which are again slightly more differentiated. Incompatible elements are very well correlated (Fig. 8). REE-chondrite normalized patterns (Evensen et al. 1978) have parallel trends (Fig. 9), with strong enrichments in

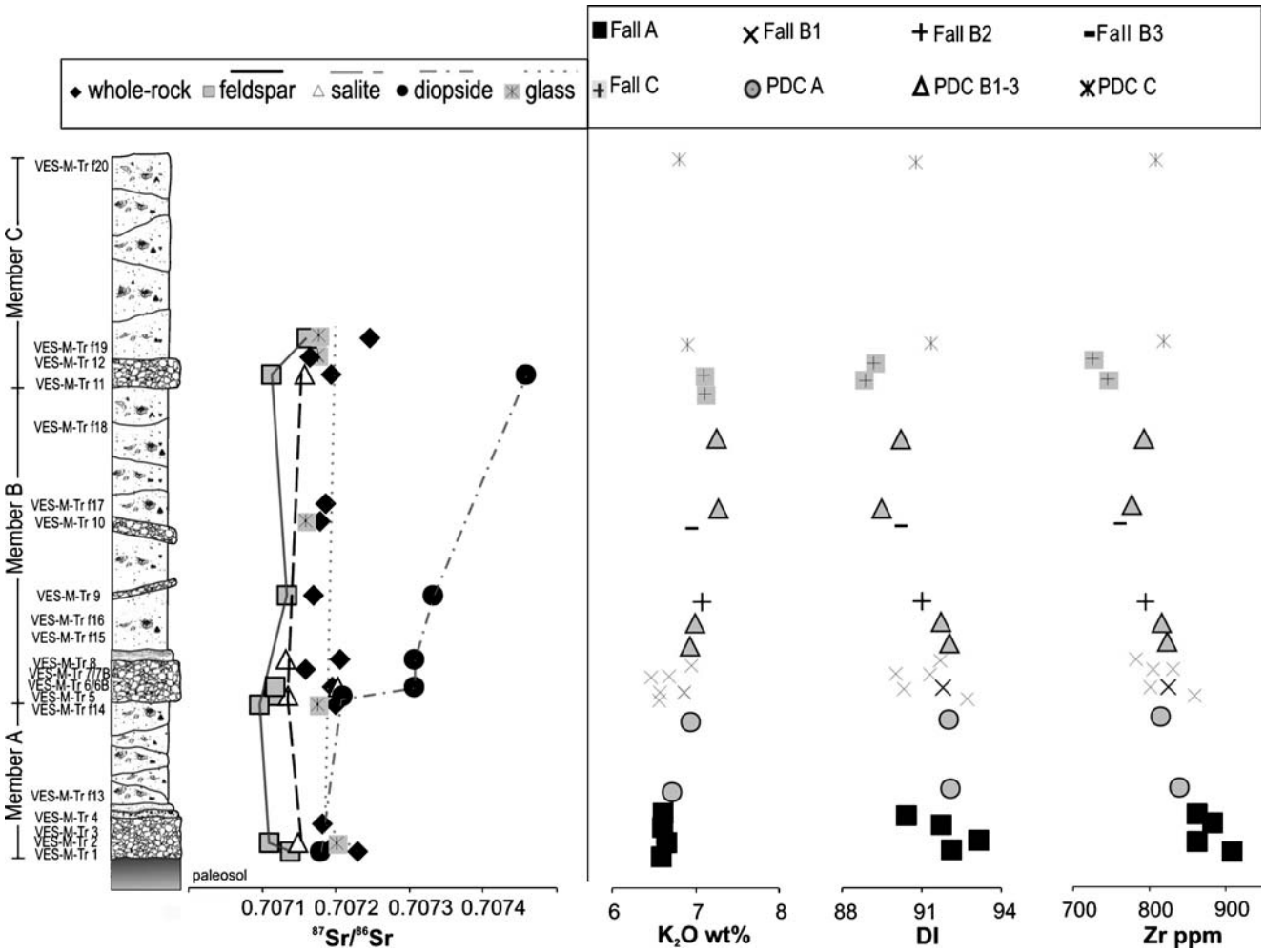

Fig. 7 Variation diagram for Sr isotopes of whole-rock, mineral phases and glass, as well as K_2O, Zr and DI along the Pomici di Mercato Tephra stratigraphic sequence. *PDC* Pyroclastic density current

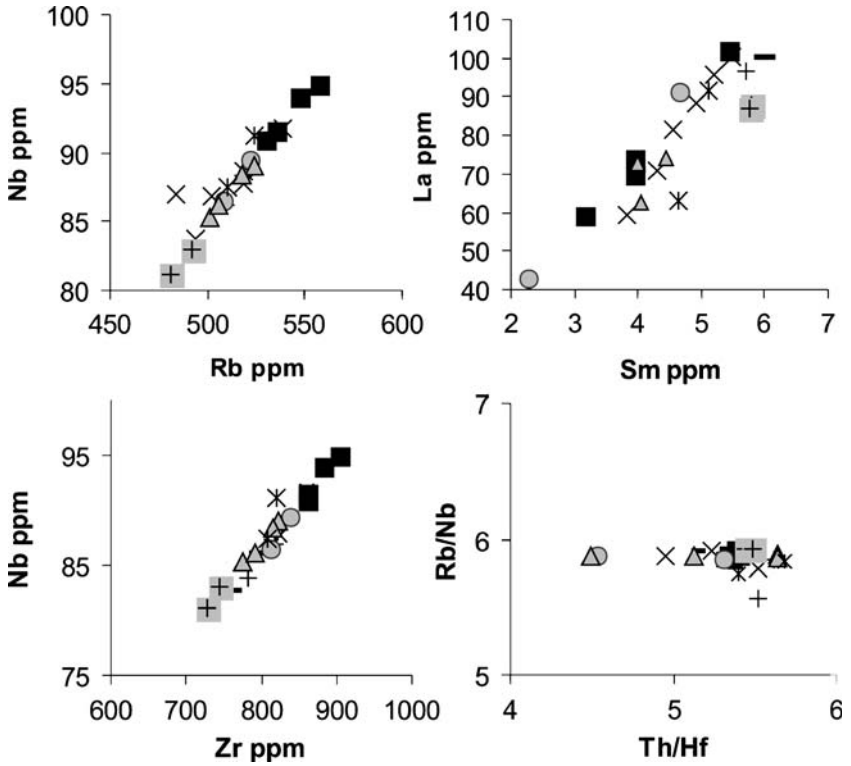

Fig. 8 Harker diagrams of representative trace elements (and ratios) as a function of trace elements (and ratios). *Symbols* as in Fig. 6

LREE with respect to HREE and with a prominent negative Eu anomaly due to feldspar fractionation (Eu/Eu* ca. 0.12). In comparison to the phonolites of the subsequent Pomici di Avellino and AD 79 eruption products, the PdM phonolites display the highest Ce/Yb ratio (>100), evidencing significant garnet fractionation.

Isotopes: $^{87}Sr/^{86}Sr$ has been measured for pumice fragments (15 analyses), for feldspar (8), diopside (6), salite (5) mineral separates, and pumice glass (8), while $^{143}Nd/^{144}Nd$ has been determined only for pumice fragments (8) (Table 6). $^{87}Sr/^{86}Sr$ and $^{143}Nd/^{144}Nd$ analyses of PdM samples were previously published by Ayuso et al. (1998), Civetta et al. (2004), Joron et al. (1987), Rolandi et al. (1993b) and Scheibner et al. (2007), who reported a few $^{87}Sr/^{86}Sr$ analyses of minerals and glass.

$^{87}Sr/^{86}Sr$ of whole-rock pumice samples varies from ca. 0.70716 to 0.70725. Feldspar is very homogeneous (ca. 0.70712) and is characterized by having the lowest isotopic values of all the analyzed mineral phases, glass, and whole rock. Sr-isotopic value of diopside varies from 0.707179±7 to 0.707458±7, with the more radiogenic values upsection. $^{87}Sr/^{86}Sr$ of salite ranges from 0.707132±6 to 0.707203±7, without any systematic variations through the sequence. Glass also shows a very restricted range of values (from 0.707158±4 to 0.707201±6). $^{143}Nd/^{144}Nd$ of all the pumice samples is very constant around 0.512470. In Fig. 7 the Sr isotopic data of whole-rock, glass, diopside and salite are reported as functions of stratigraphic position. In comparison to the other Vesuvian-Plinian and sub-Plinian eruptions (Pomici di Base, Pomici Verdoline, Pomici di Avellino, AD 79, AD 472, and AD 1631) the PdM products show (glass and whole rock) the most restricted range of isotopic values, with only feldspar and diopside significantly in disequilibrium with glass in the last erupted products.

Discussion and conclusions

The sedimentological and textural characteristics of the PdM sequence (Fig. 4) may suggest that the eruption took

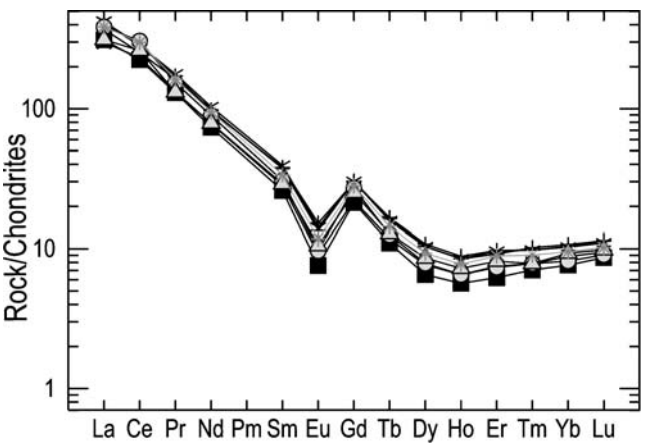

Fig. 9 Chondrite-normalized rare earth pattern for representative samples of Pomici di Mercato Tephra

Table 6 Sr and Nd isotopic ratios of selected whole rock, glass and minerals from Pomici di Mercato Tephra

Sample	Layer	$^{87}Sr/^{86}Sr$ Pumice	$^{143}Nd/^{144}Nd$ Pumice	$^{87}Sr/^{86}Sr$ Feldspars	$^{87}Sr/^{86}Sr$ Diopside	$^{87}Sr/^{86}Sr$ Salite	$^{87}Sr/^{86}Sr$ Glass	$^{87}Sr/^{86}Sr$ Single pumice glass
VES-M-TR1	Fall A	0.707229±5		0.707138±7	0.707179±7			
VES-M-TR2	Fall A	0.707193±5		0.707109±9		0.707148±6	0.707201±6	0.707158±4
VES-M-TR3	Fall A	0.707182±6	0.512470±4					
VES-M-TR5	Fall B1	0.707210±8	0.512477±8	0.707115±5	0.707208±5	0.707135±5		
VES-M-TR6	Fall B1	0.707195±8	0.512473±3	0.707121±5	0.707306±8	0.707203±7		
VES-M-TR7	Fall B1	0.707159±12						
VES-M-TR8	Fall B1	0.707205±8	0.512478±8		0.707306±7	0.707132±6		
VES-M-TR9	Fall B2	0.707170±6		0.707134±6	0.707332±5			
VES-M-TR10	Fall B3	0.707178±6					0.707159±7	0.707169±5
VES-M-TR11	Fall C	0.707194±21		0.707113±6	0.707458±7	0.707157±7		
VES-M-TR12	Fall C	0.707168±7					0.707176±5	0.707162±6
VES-M-TRf14	PDC A	0.707199±7	0.512465±8	0.707096±8			0.707175±8	
VES-M-TRf16	PDC B1		0.512480±7					
VES-M-TRf17	PDC B2	0.707186±6						
VES-M-TRf19	PDC C	0.707246±6		0.707161±12			0.707176±9	
VES-M-TRf20	PDC C		0.512469±7					

PDC Pyroclastic density current. The quoted error (2σ) refers to the last digit

place through a fairly continuous process. The absence in the sequence of erosional unconformities or reworked deposits is evidence for any significant break in the activity. Furthermore, lack of any dramatic variation in the lithological characteristics of the entire sequence, excludes occurrence of both significant changes in eruption dynamics and volcano-tectonic events. The eruption was likely dominated by magmatic explosions feeding a pulsating and progressively higher column, which was affected by three major collapses, each generating dense pyroclastic currents.

The erupted phonolitic magma shows a narrow range of major and trace elements compositions. Least-squares mixing calculations (Stormer and Nicholls 1978) show that the transition from the least to the most differentiated magma would be accommodated by a 27% subtraction of sanidine (66%) and salite (34%) and an 8% addition of plagioclase (21%) and diopside (79%). This result is in agreement with trace element Rayleigh fractionation modeling results. These computations show that fractional crystallization does not account for the detected chemical variations and mineralogical assemblage and suggest an open-system behaviour. The measured isotopic disequilibria and the mineral chemistry also support such a hypothesis. In fact, feldspar and diopside, contrary to salite, are not in isotopic equilibrium with glass (Fig. 7). Furthermore, the mineral chemistry shows disequilibrium between plagioclase and sanidine and coexistence of two pyroxenes of different composition (salite to Fe-salite, and diopside). The isotopic and mineralogical data, as well as the results of major-element modeling, show that diopside and plagioclase have not crystallized from the PdM magma. They strongly suggest that these minerals are xenocrysts, probably left along the chamber wall by earlier magmas.

The homogeneity of the isotopic composition of the pumice glass, the isotopic equilibrium between glass and salite, and the narrow compositional range of pumice, resulting from fractional crystallization and xenocrysts entrainment, further support lack of pre- and syn-eruptive mixing-mingling processes among isotopically and chemically distinct magma batches. Entrainment of diopside and plagioclase xenocrysts is the only open-system process operating within the PdM chamber. This is a major difference with respect to the other Vesuvian-Plinian and sub-Plinian eruptions, which are all characterized by chemical zoning of the erupted products, and by a systematic isotopic variation in the magmas extruded during the course of the eruption (e.g., Civetta et al. 1991; Civetta and Santacroce 1992; Cioni et al. 1995).

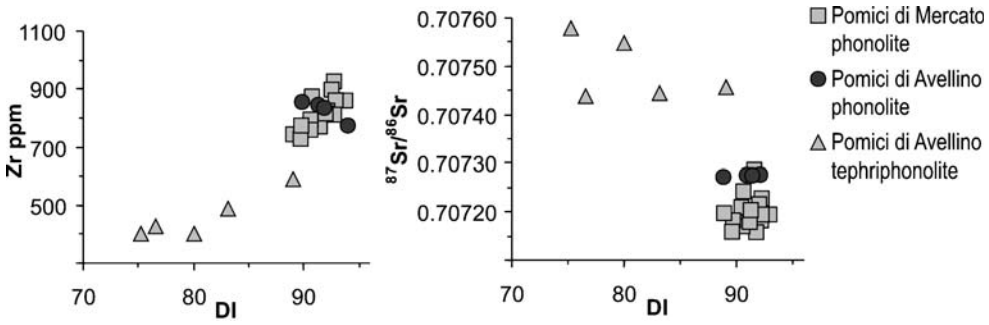

Fig. 10 Variation diagrams of Zr and $^{87}Sr/^{86}Sr$ as a function of DI. Data for Pomici di Avellino from Civetta et al. (1991), and Civetta (unpublished data)

The question why the PdM magma chamber is fairly compositionally and isotopically homogenous, unlike the other Vesuvian eruptions, remains. Our explanation implies that the phonolitic PdM magma is a portion of a larger isotopically homogeneous phonolitic magma reservoir, not refilled by less evolved melts during differentiation of the PdM phonolitic magma. Only after the PdM eruption, new and less differentiated magma, entered the chamber, differentiated and mixed with the residual PdM magma, to form a compositionally and isotopically zoned reservoir, characterized by a layered phonolitic upper part and an homogeneous tephriphonolitic lower portion that fed the subsequent Pomici di Avellino eruption (3780±70 a).

This hypothesis is supported by the similarity in chemistry and isotopes (Fig. 10) between the PdM phonolite and the first-erupted Pomici di Avellino phonolite. In fact, they are highly evolved and are the only Vesuvian products with Na_2O/K_2O ratio higher than 1; both are characterized by similar REE pattern, with high fractionated Ce/Yb ratio compared to all the other volcanic products of Vesuvius (Scheibner et al. 2007), and by similar Sr- Nd-isotopes (this paper and Civetta et al. 1991). Furthermore the PdM and the Pomici di Avellino phonolites and tephriphonolites describe a unique compositional and isotopic trend (Fig. 10). This hypothesis is also corroborated by the occurrence of equilibrium unzoned garnets within the PdM phonolite and disequilibrium zoned garnets within the Pomici di Avellino phonolite, the latter explained as due to refilling of the residual PdM magma chamber by the less-differentiated tephriphonolitic Pomici di Avellino magma (Scheibner et al. 2007). It is in full agreement with the similar pressure estimates for both PdM and Pomici di Avellino magma chambers (about 200±20 MPa, Scaillet and Pichavant 2004), and fits well into the general model presented by Santacroce et al. (1994) of how Vesuvius works.

Acknowledgments This project was carried out within the framework of the EU Research Training Network HPRN-CT-2000–00060, the EU EVG1-CT-2002–00058 ERUPT, the Spanish REN2002–10877-E/RIES project, the 2006BE–00549 fellowship and the INGV-DPC Vesuvius projects. The authors thank Dan Morgan, Raffaello Cioni, two anonymous referees, and Massimo D'Antonio for their scientific support, and Antonio Carandente and Pasquale Belviso from Istituto Nazionale di Geofisica e Vulcanologia – Sezione di Napoli "Osservatorio Vesuviano" and all the staff of Serveis Cientifico Tecnics of Universitat de Barcelona for their skilled technical support.

References

Andronico D, Calderoni G, Cioni R, Sbrana A, Sulpizio R, Santacroce R (1995) Geological map of Somma-Vesuvius volcano. Per Mineral 64(1–2):77–78

Arnó V, Principe C, Rosi M, Santacroce R, Sbrana A, Sheridan MF (1987) Eruptive history. In: Santacroce R (Ed) Somma-Vesuvius. Quaderni de "La Ricerca Scientifica" CNR, Roma 114:53–103

Auger E, Gasparini P, Virieux J, Zollo A (2001) Seismic evidence of an extended magmatic sill under Mt. Vesuvius. Science 294:1510–1512

Ayuso RA, De Vivo B, Rolandi G, Seal II RR, Paone A (1998) Geochemical and isotopic variations bearing on the genesis of volcanic rock from Vesuvius, Italy. J Volcanol Geotherm Res 82:53–78

Barberi F, Bizouard H, Clocchiatti R, Métrich N, Santacroce R, Sbrana A (1981) The Somma-Vesuvius magma chamber: a petrological and volcanological approach. Bull Volcanol 44:295–315

Belkin HE, De Vivo B, Roedder E, Cortini M (1985) Fluid inclusion geobarometry from ejected Mt. Somma-Vesuvius nodules. Am Mineral 70:288–303

Belkin HE, Kilburn RJ, De Vivo B (1993) Fluid inclusions studies of ejected nodules from Plinian eruptions of. Mt. Somma-Vesuvius. J Volcanol Geotherm Res 58:89–100

Bianco F, Castellano M, Milano G, Ventura G, Vilardo G (1998) The Somma-Vesuvius stress fields induced by regional tectonics: evidences by seismological and mesostructural data. J Volcanol Geotherm Res 82:199–218

Brocchini D, Principe C, Castradori D, Laurenzi MA, Gorla L (2001) Quaternary evolution of the southern sector of the Campanian Plain and early Somma-Vesuvius activity: insights from Trecase 1 well. Mineral Petrol 73:67–91

Caprarelli G, Togashi S, De Vivo B (1993) Preliminary Sr and Nd isotopic data for recent lavas from Vesuvius volcano. J Volcanol Geotherm Res 58:377–381

Cioni R, Civetta L, Marianelli P, Metrich N, Santacroce R, Sbrana A (1995) Compositional layering and syn-eruptive mixing of a periodically refilled shallow magma chamber: the AD 79 Plinian eruption of Vesuvius. J Petrol 36:739–776

Cioni R, Santacroce R, Sbrana A (1999) Pyroclastic deposits as a guide for reconstructing the multi-stage evolution of the Somma-Vesuvius caldera. Bull Volcanol 61:207–222

Cioni R, Longo A, Macedonio G, Santacroce R, Sbrana A, Sulpizio R, Andronico D (2003) Assessing pyroclastic fall hazard through field data and numerical simulations: Example from Vesuvius. J Geophys Res 108(B2), 2063 DOI 10.1029/2001JB000642

Civetta L, Santacroce R (1992) Steady state magma supply in the last 3400 years of Vesuvius activity. Acta Vulcanol 2:147–159

Civetta L, D'Antonio M, Paone E, Santacroce R (1987) Isotopic studies of the products of 472 AD Pollena eruption (Somma-Vesuvius). Boll GNV III:263–271

Civetta L, Galati R, Santacroce R (1991) Magma mixing and convective compositional layering within the Vesuvius magma chamber. Bull Volcanol 53:287–300

Civetta L, D'Antonio M, de Lorenzo S, Di Renzo V, Gasparini P (2004) Thermal and geochemical constraints on the 'deep' magmatic structure of Mt. Vesuvius. J Volcanol Geotherm Res 133:1–12

Delibrias G, Di Paola GM, Rosi M, Santacroce R (1979) La storia eruttiva del complesso vulcanico Somma-Vesuvio ricostruita dalle successioni piroclastiche del Monte Somma. Rend Soc It Min Petrol 35(1):411–438

Deines P, Goldstein SL, Oelkers EH, Rudnick RL, Walter LM (2003) Standards for publication of isotope ratio and chemical data in chemical geology. Chem Geol 202 (1):1–4

de Lorenzo S, Di Renzo V, Civetta L, D'Antonio M, Gasparini P (2006) Thermal model of the Vesuvius magma chamber. Geophys Res Lett 33, L17302, DOI 10.1029/2006GL026587

Diaz N, Garcia-Veigas J, Gimeno D (1996) Desarrollo de una metodología de análisis de vidrios volcánicos ácidos, y sus equivalentes desvitrificados, por microsonda electrónica. Bol Soc Esp Mineralogía 21–A:74–75

Di Renzo V, Di Vito MA, Arienzo I, Civetta L, D'Antonio M, Giordano F, Orsi G, Tonarini S (2007) Magmatic history of

Somma-Vesuvius on the basis of new geochemical and isotopic data from a deep borehole (Camaldoli della Torre). J Petrol 48:753–784

Evensen NM, Hamilton PJ, O'Nions RK (1978) Rare earth abundances in chondritic meteorites. Geochim Cosmochim Acta 42(8): 1199–1212

Fulignati P, Marianelli P, Sbrana A (1998) New insights on the thermometamorphic-metasomatic magma chamber shell of the 1944 eruption of Vesuvius. Acta Vulcanol 10:47–54

Joron JL, Métrich N, Rosi M, Santacroce R, Sbrana A (1987) Chemistry and petrography. In: Santacroce R (Ed) Somma-Vesuvius. Quaderni de "La Ricerca Scientifica" CNR, Roma 8:105–171

Landi P, Bertagnini A, Rosi M (1999) Chemical zoning and crystallisation mechanisms in the magma chamber of the Pomici di Base Plinian eruption of Somma-Vesuvius (Italy). Contrib Mineral Petrol 135 (23):179–197

Le Bas MJ, Le Maitre RW, Streckeisen R, Zanettin B, Bellieni G (1986) A chemical classification of volcanic rocks based on total alkali-silica diagram. J Petrol 27:745–750

Lima A, Danyushevsky LV, De Vivo B, Fedele L (2003) A model for the evolution of the Mt. Somma-Vesuvius magmatic system based on fluid and melt inclusion investigations. In: De Vivo B, Bodnar RJ (eds) Melt inclusions in volcanic system. Elsevier, Amsterdam, pp 227–249

Marianelli P, Métrich N, Santacroce R, Sbrana A (1995) Mafic magma batches at Vesuvius: a glass inclusion approach to the modalities of feeding stratovolcanoes. Contrib Mineral Petrol 120:159–169

Marianelli P, Métrich N, Sbrana A (1999) Shallow and deep reservoirs involved in magma supply of the 1944 eruption of Vesuvius. Bull Volcanol 61:48–63

Marianelli P, Sbrana A, Métrich N, Cecchetti A (2005) The deep feeding system of Vesuvius involved in recent violent strombolian eruptions. Geophys Res Lett 32:1–4

Middlemost EAK (1989) Iron oxidation ratios, norms and the classification of volcanic rocks. Chem Geol 77:19–26

Morgan DJ, Blake S, Rogers NW, De Vivo B, Rolandi G, Davidson JP (2006) Magma recharge at Vesuvius in the century prior to the eruption of AD 79. Geology 34:845–848

Piochi M, Ayuso RA, De Vivo B, Somma R (2006) Crustal contamination and crystal entrapment during polybaric magma evolution at Mt. Somma-Vesuvius volcano, Italy. Geochemical and Sr isotope evidence. Lithos 86(3–4):303–329

Orsi G, de Vita S, Di Vito M, Nave R, Heiken G (2003) Facing volcanic and related hazards in the Neapolitan area. In: Heiken G, Fakundiny R, Sutter J (eds) Earth Sciences in the Cities: a reader. AGU Sp Publ Series Washington; DC 56:121–170

Orsi G, Di Vito MA, Isaia R (2004) Volcanic hazard assessment at the restless Campi Flegrei caldera. Bull Volcanol 66:514–530

Rolandi G, Mastrolorenzo G, Barrella AM, Borrelli A (1993a) The Avellino Plinian eruption of Somma-Vesuvius (3760 y BP): the progressive evolution from magmatic to hydromagmatic style. J Volcanol Geotherm Res 58:67–88

Rolandi G, Maraffi S, Petrosino P, Lirer L (1993b) The Ottaviano eruption of Somma-Vesuvio (8000 y BP): a magmatic alternating fall and flow-forming eruption. J Volcanol Geotherm Res 58:43–65

Santacroce R (1983) A general model for the behaviour of the Somma-Vesuvius volcanic complex. J Volcanol Geotherm Res 17:237–248

Santacroce R (Ed) (1987) Somma-Vesuvius. Quaderni de "La Ricerca Scientifica" CNR, Roma 114(8):230

Santacroce R, Sbrana A (eds) (2003) Geological Map of Vesuvius. SELCA (FI)

Santacroce R, Bertagnini A, Civetta L, Landi P, Sbrana A (1993) Eruptive dynamics and petrogenetic processes in a very shallow magma reservoir: the 1906 eruption of Vesuvius. J Petrol 34:383–425

Santacroce R, Cioni R, Civetta L, Marianelli P, Métrich N (1994) How Vesuvius works. Atti Conv Lincei 112:185–196

Santacroce R, Cioni R, Marianelli P, Sbrana A (2005) Understanding Vesuvius and Preparing for its Next Eruption. In: Balmuth MS, Chester DK, Johnston PA (eds) Cultural Responses to the Volcanic Landscape. Archaeological Institute of America, pp 27–55

Scaillet B, Pichavant M (2004) Crystallisation conditions of Vesuvius phonolites. Geophys Res Abstr 6:03764

Scheibner B, Wörner G, Civetta L, Simon K, Kronz A (2007) Rare earth element fractionation in magma Ca-rich garnets. Contrib Mineral Petrol (in press)

Somma R, Ayuso RA, De Vivo B, Rolandi G (2001) Major, trace elements and isotope geochemistry (Sr-Nd-Pb) of interplinian magmas from Mt. Somma-Vesuvius (southern Italy). Mineral Petrol 73:121–143

Stormer JC, Nicholls J (1978) XLFRAC: a program for interacting testing of magmatic differentiation models. Comp Geosci 4:143–159

Thornton CP, Tuttle OF (1960) Chemistry of igneous rocks: 1. Differentiation Index. Am J Sci 258:664–684

Ventura G, Vilardo G (1999) Seismic-based estimate of hydraulic parameters at Vesuvius volcano. Geophys Res Lett 26(7):887–890

Walker GPL (1977) Metodi geologici per la valutazioni del rischio vulcanico. Atti Conv I vulcani attivi dell'area napoletana. Regione Campania, Napoli, pp 53–60

Wilson L, Sparks RSJ, Walker GPL (1980) Explosive volcanic eruptions – IV. The control of magma properties and conduit geometry on eruption column behaviour. Geophys J R Astr Soc 63:117–148

Zollo A, Gasparini P, Virieux J, le Meur H, de Natale G, Biella G, Boschi E, Capuano P (1996) Seismic evidence for a low-velocity zone in the upper crust beneath mount Vesuvius. Science 274:592–594